1 Forze Entropiche

2 Ideal gas expansion

All of you are familiar with the ideal gas model. The Hamiltonian of this system of N identical particles of mass m in a volume V is quite simple, coinciding with the classical kinetic energy

$$H = \sum_{i=1}^{N} \frac{p_i^2}{2m}$$

The corresponding partition function in the Canonical ensemble is

$$Q = \frac{1}{N!h^{3N}} \int d\mathbf{r}_1 ... d\mathbf{r}_N d\mathbf{p}_1 ... d\mathbf{p}_N e^{-\beta H} = \frac{1}{N!h^{3N}} V^N \left[\int dp_x e^{-\beta p_x^2/2m} \right]^{3N}$$

$$= \frac{1}{N!h^{3N}} V^N (\sqrt{2\pi m k_B T})^{3N}$$

defining $\lambda^{-1} = \frac{\sqrt{2\pi m k_B T}}{h}$,

$$Q = \left(\frac{V}{\lambda^3} \right)^N$$

The log of the partition function provides the system Helmholtz free energy F, which in this case is

$$F = -k_B T \ln Q$$

from which one can evaluate the well known ideal gas equation of state $P(V,T)$ as

$$P = -\frac{\partial F}{\partial V} = k_B T \frac{\partial \ln Q}{\partial V} = k_B T N \frac{\partial \ln V}{\partial V} = k_B T \frac{N}{V}$$

An ideal gas, in a container with a mobile piston, will then extern a force on the piston proportional to the gas concentration. Despite you may not have thought in this way, the ideal gas provides a very basic example of an entirely entropic force controlling the evolution of the system.

3 Equilibrium osmotic pressure obeys the ideal gas law - Nelson

We can now turn to the problem of osmotic pressure. A membrane divides a rigid container into two chambers, one with pure water, the other containing a dilute solution of N solute particles in volume V. The solute could be anything from individual molecules (sugar) to proteins, to colloidal particles. We suppose the membrane to be permeable to water but

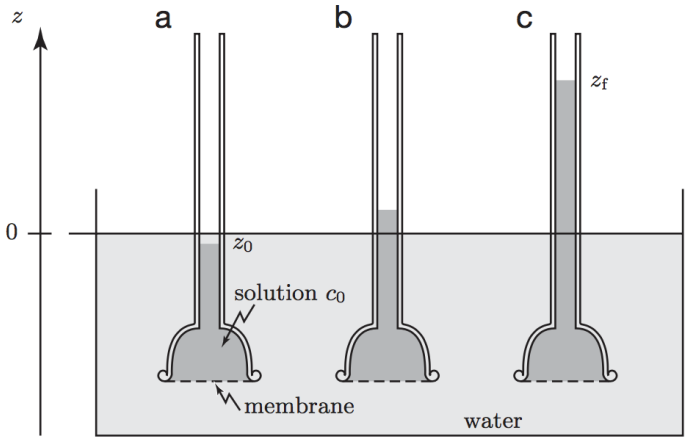

Figure 7.1: (Schematic.) (a) A semipermeable membrane is stretched across a cup-shaped vessel containing sugar solution with concentration c_0. The vessel is then plunged into pure water. Initially the sugar solution rises to a height z_0 in the neck of the cup. (b) Solution begins to rise in the vessel by osmotic flow, until (c) it reaches an equilibrium height z_f. The pressure in the final equilibrium state is the final height z_f times $\rho_{m,w}g$.

Figure 1: Note that if one integrate $\rho g dz$ in the water sample one finds at the bottom $\rho g h_1$. If one integrate (panel c) inside the cup, one find $\rho g h_1 + \rho g h_2$. Thus, across the membrane there is a pressure difference equal to $\rho g h_2$. Here h_1 is the depth of the cup, h_2 is the upper height of the solution in the cup.

not to solute. A very literal example would be an ultrafine sieve, with pores too small to pass solute particles. The system will come to an equilibrium with greater hydrostatic pressure on the sugar side, which we measure (see figure).

We would like a quantitative prediction for this "osmotic pressure." One might think that the situation just described would be vastly more complicated than the ideal-gas problem. After all, the solute molecules are in the constant, crowded, company of water molecules. It is true that the solute molecules interact strongly with the water, and the water molecules with each other. But in a dilute solution the solute particles don't interact much with each other, and so the total energy of a microstate is unaffected by their locations. More precisely, the integral over the positions of the solute molecules is dominated by the large domain where no two are close enough to interact significantly. (This approximation breaks down for concentrated solutions, just as the ideal gas law fails for dense gases.)

This means that if we calculate the partition function of both solute and solvent particles we need to write

$$Z = \int d\mathbf{r_1}...d\mathbf{r_N}d\mathbf{r_1^w}...d\mathbf{r_{N_w}^w}e^{-\beta[U_{ww}(\mathbf{r^w})+U_{ws}(\mathbf{r^w},(\mathbf{r})]}$$

Assuming each solute is solvated by some water particles, then we can approximate $U_{ws}(\mathbf{r^w},\mathbf{r}) = Nu_0$, where u_0 is the solvation energy. Then

$$Z = e^{-\beta N u_0}\int_V d\mathbf{r_1}...d\mathbf{r_N}\int d\mathbf{r_1^w}...d\mathbf{r_{N_w}^w}e^{-\beta[U_{ww}(\mathbf{r^w})]}$$

Thus for dilute solutions we can do all the integrals over the solute particle locations and we get V^N, where V is the volume of just that part of the chamber accessible to solute. The factorization we have used is consistent with the assumption that the membrane is essentially invisible to water molecules. Hence, the V derivative of the remaining part is nothing more then the pressure of a system with no solutes, the pure water pressure P_W. The total pressure is thus the sum of two terms, P_W and the equilibrium osmotic pressure Π given by the ideal gas law:

$$\Pi = \frac{N}{V}RT$$

Here $c = N/V$ is the number density of solute molecules. Π is the force per area that we must apply to the solute side of the apparatus in order to get equilibrium. The discussion above was appropriate to the situation of a horizontal chamber separated by a membrane. In the more common situation shown in the Figure, we again get a relation for the difference in pressure between the two sides of the membrane. This difference in pressure must compensate the difference in height of the sample. Thus

$$\Pi = \rho g z_f$$

where z_f is the final height of the column of fluid, ρ is the mass density of water, and g is the acceleration of gravity. Thus in this case we conclude that the equilibrium height of the fluid column is proportional to the solute concentration in the cup (after dilution).

Note that one could think of using the rise of the column to lift a weight. Then one could extract energy from the dilution process taking place when salty and still water are mixed together, like at the river's estuary. There are groups working on this idea.

3.0.1 Relevance of Π to cells

We need some estimates to see if osmotic pressure is really significant in the world of the cell. Suppose a cell contains globular proteins, roughly spheres of radius 10nm, at a concentration such that 30% of the cell's volume is occupied with protein (we say that the volume fraction ϕ is equals to 0.3). This is not an unreasonable picture of red blood cells, which are stuffed with hemoglobin. To find the concentration c, we set 0.3 equal to the number of proteins per volume times the volume of one protein:

$$\phi = \frac{N}{V}\frac{\pi}{6}\sigma^3 \quad \rightarrow \quad 0.3 = c\frac{\pi}{6}20^3\ 10^{-27}$$

Thus $c \approx 7\ 10^{22}$ m^{-3}. To phrase this in more familiar units, remember that one mole per liter corresponds to a concentration of $6\ 10^{23}/10^{-3}$ m^{-3}. We'll call a solution of 1 mole/L a one molar solution, defining the symbol M = mole/L, so we have a solution with $c = 1.2\ 10^{-4}$ M or a 0.12 mM solution. In this class we will pretend that dilute-solution formulas are always applicable, and so will not distinguish between molar and molal concentration.

The osmotic pressure needed to keep our protein solution inside a cell, with pure water outside, is then $k_B T_r c \approx 300Pa$. That's certainly much smaller than atmospheric pressure (10^5 Pa), but is it big for a cell? In other words, what is the surface tension that the membrane must be able to provide to avoid the rupture of the membrane (assumed to be permeable to water) ?

The surface tension γ times the surface A is defined as the energy associated to the interface (the membrane). Its derivative gives the force that the interface applies on the confining volume. For a spherical droplet, $A = 4\pi R^2$ and

$$F = -\frac{d\gamma A}{dR} = -\gamma 8\pi R$$

Similarly, the confined fluid applies to the membrane a force attempting to expand the interface equal to

$$F = \Pi A = 4\pi R^2 \Pi$$

At equilibrium

$$\gamma = \frac{R\Pi}{2}$$

Suppose now that the cell has radius $R = 10\mu m$ and that the osmotic pressure creates an excess internal pressure of $300Pa$. Then, the requested surface tension must be

$$\gamma = 10^{-5}m \cdot 300 \cdot 2 \text{ Pa} \quad = 6 \cdot 10^{-3} \text{ N/m}$$

This surface tension value turns out to be roughly enough to rupture a eukaryotic cell membrane, destroying the cell. **Osmotic pressure is thus significant for cells**.

The situation is even more serious with a small solute like salt. Bilayer membranes are only slightly permeable to sodium and chloride ions. A 1 M salt solution contains about 10^{27} ions per m^3, ten thousand times more than in the protein example above! And indeed it's well known that you cannot dilute red blood cells with pure water; at low concentrations of exterior salt they burst, or lyse. Clearly to escape lysis, living cells must precisely fine-tune their concentrations of dissolved solutes.

4 Hard Sphere Crystallization

In January 1957 in New Jersey during a symposium on many body problems, Alder and Wainwright presented their first results on molecular dynamics simulations of hard spheres (HS), suggesting the possibility of a transition toward an ordered crystalline phase on increasing the density of the HS fluid. George Uhlenbeck, during the discussion time, asked the participants to express their personal feeling on such a possibility and the vote ended up even. The cartoon in Fig. 2-(b) and the commonly but improperly assumed connection between entropy and disorder possibly explain the difficulty of reaching a consensus on this question. Hard spheres interact only via excluded volume, preventing any pair of particles to become closer than their diameters (Fig. 2-(a)). No energy is involved in the interaction. Thus, thermodynamic is fully controlled by the entropic term in the free energy. Improperly, the possibility of hard-sphere crystallization was perceived as contradicting the meaning of entropy as a driving force toward increasing disorder. How can a crystal be more disordered than a fluid configuration?

To properly answer the question, one needs to consider the number of microstates explored in the fluid and in the crystal phase. In the crystal, particles move in cages provided by their own neighbours, as vividly shown in the cathode-ray tube used by Alder and Wainwright to visualize the molecular dynamics trajectories of two-dimensional crystalline hard-disks (Fig. 2-(d)). The width of the spots created by the bright line paths is a visual measure of the phase-space sampled by each particle. The log of the number of sampled microstates constitutes the entropy of the crystal, which we can name vibrational or cage entropy. In the fluid, we can distinguish two contributions to the entropy: a vibrational contribution, which again depends on the available volume inside the cage and a second contribution which measures the number of different disordered arrangements of the particles, commonly named as configurational entropy. The mean square displacement (MSD) of

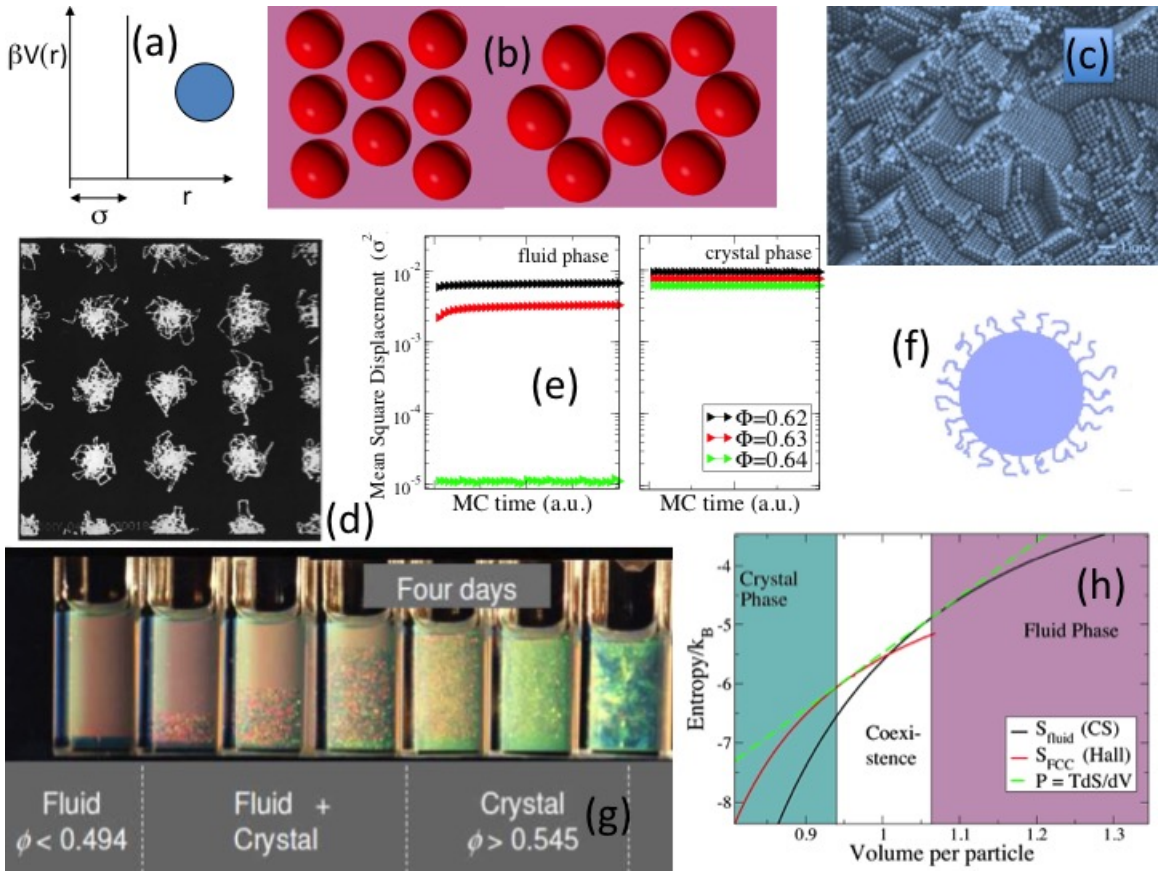

Figure 2: The hard-sphere model. (a) The radial dependence of the interaction potential, $\beta V(r)$. The potential is infinite for r smaller than the particle diameter and zero everywhere else. (b) A cartoon of a crystalline and of a fluid configuration to highlight the different order perceived by our eyes, trained to capture only the configurational part of the entropy. (c) An electron microscope image of a colloidal crystal (courtesy of D. Pine). The particles in the photograph are made from polystyrene, a common commercial plastic. Notice that there are both hexagonal and square planes visible, which is consistent with a face-centered cubic lattice. (d) The original trajectories detected in the first molecular dynamics calculation of hard disks as shown by the cathode-ray tube used by Alder and Wainwright. (e) A comparison between the mean square displacement of HS particles in the fluid and in the crystal phase. In the crystal phase, particles rattle in larger cages, a confirmation of the larger vibrational entropy. (f) A cartoon of a polymer-grafted colloid. (g) The fluid, coexisting and crystal phases observed in the classic experiment by Pusey and van Megen (h) The volume dependence of the fluid and crystal entropy (with an arbitrary additive constant) as predicted by the CS and the Hall equation of state. The dashed line is tangent to both the fluid and the crystal entropy. Since $P = TdS/dV$, the two tangent points indicate two volumes V_{xt} and V_{fluid} for which both temperature and pressure are identical. If we further indicate with S_0 the intercept of the same line at zero volume, then we can write for these two points $S = S_0 + VdS/dV = S_0 + PV/T$. Then the Gibbs free energy per particle $G/N = (-TS + PV)/N$ is equal to $-TS_0/N$ for both V_{xt} and V_{fluid}, proving that these two volumes have also the same chemical potential $\mu \equiv G/N$. Thus, V_{xt} and V_{fluid} are two coexisting phases.

a particle in the dense fluid or in the crystal can be considered as a proxy for the vibrational contribution to entropy. Fig. 2-(e) contrasts the MSD in disordered and ordered dense HS configurations to provide evidence that the phase-space volume explored by the particles in the cage (vibrational motion) is significantly smaller in disordered configurations. The difference in vibrational entropy can be so large that the additional configurational contribution is not any longer sufficient to thermodynamically stabilise the fluid phase. The ordered crystal has a larger entropy than the fluid.

Quite accurate estimates of the HS entropy are nowadays available. The fluid phase entropy per particle can be approximated with the Carnahan-Starling (CS) expression (slightly more accurate expressions as the one by Kolafa are available)

$$\frac{1}{N}\frac{S_{ex}^{CS}}{k_B} = -\frac{4\phi - 3\phi^2}{(1-\phi)^2}, \tag{1}$$

where ϕ is the packing fraction. The face-centered cubic (FCC) crystal free energy can be approximated using Hall expression, a phenomenological expression based on computer simulation results. Hall noted that the compressibility factor Z_{HS} of the FCC HS crystal can be quite accurately modelled by

$$Z_{HS} = \frac{\beta P}{\rho} = \frac{1 + \phi + \phi^2 - 0.67825\phi^3 - \phi^4 - 0.5\phi^5 - 6.028\phi^6 f(\phi)}{1 - 3\phi + 3\phi^2 - 1.004305\phi^3}, \tag{2}$$

with $f(\phi) = \exp((\pi\sqrt{2}/6 - \phi)[7.9 - 3.9(\pi\sqrt{2}/6 - \phi)])$. In order to calculate the excess entropy S^{ex} per particle from the compressibility factor Z_{HS}, a thermodynamic integration in ϕ can be performed, obtaining

$$\frac{S^{ex}(\phi)}{Nk_B} = \frac{S^{ex}(\phi^*)}{Nk_B} - \int_{\phi^*}^{\phi} \left(\frac{\beta P}{\rho} - 1\right) \frac{d\phi'}{\phi'} \tag{3}$$

The integration in Eq. 3 is usually started from $\phi^* = 0.544993$, a value for which an accurate estimate of the excess crystal entropy $\frac{S^{ex}(\phi^*)}{k_B} = -5.91889$ based on computer simulation is available.

Fig. 2-(h) shows the fluid and crystal entropy per particle as a function of the volume per particle for the HS system. In the case of hard bodies, the free energy F has only the entropic contribution $F = -TS$. Thus the pressure, the volume derivative of the free energy, is $P = T\partial S/\partial V|_T$. The pressure is thus nothing more than the derivative of the entropy function reported in Fig. 2-(h). Hence, the common tangent line shown in Fig. 2-(h) identifies two phases (fluid and crystal) with the same T, P and identical chemical potential μ (being $\mu = (F + PV)/N$, see caption of Fig. 2). The equality of T, P and μ sets the condition for phase-coexistence. In the region between the two coexisting phases, in the thermodynamic limit, entropy is maximised by the presence of two coexisting phases.

5 Depletion Interactions:

Now we turn to an important entropic interaction, called depletion interaction. Such interaction, being attractive, promote the formation of dense phases, e.g. macromolecule or particle association. To start with, let's try to answer to the following question: if I have two large hard-spheres in a solution of small hard-spheres, will the two large spheres attract ? The answer to this question is at the hearth of the entropic interactions.

5.1 Depletion Interactions: Theory

One of the most powerful ways to control the attractive interaction between hard bodies is provided by the so-called depletion interaction.The addition in solution of small (compared to the colloids) non-absorbing cosolutes (i.e. non interacting with the particles, apart from the excluded volume) induces an entropic attraction between the colloids proportional to a first approximation to the concentration of cosolutes. The physics behind this important attractive interaction was clarified by two Japanese polymer scientists, Asakura and Oosawa, in a study which has remained unnoticed for more than two decades before becoming a seminal contribution.

Asakura and Oosawa proposed to focus on an idealized model, i.e. two large hard particles of diameter σ_c (the colloids) in the presence of M small hard particles (the depletants) of diameter σ_p in a volume V (Fig. 3-(a-b)). They derived the statistical mechanics description of the system to evaluate the probability to find the two colloids at relative distance r, under the simplifying assumption that the depletants do not interact among themselves (an ideal gas) but do interact via excluded volume with the two colloids.

Indicating with $\vec{r}$ and $\vec{s}$ the positions of the colloids and of the cosolutes, the partition function in the canonical ensemble can be written as

$$Q = \frac{1}{2\lambda_1^6}\frac{1}{M!\lambda_2^{3M}}\int e^{-\beta(V_{11}(\vec{r}_1,\vec{r}_2)}d\vec{r}_1 d\vec{r}_2 \int d\vec{s}_1 ... d\vec{s}_M e^{-\beta V_{12}(\vec{r}_1,\vec{r}_2,\vec{s}^M)}, \tag{4}$$

where V_{11} is the HS potential between the colloids and V_{12} the HS potential between the depletants and the two colloids. Since V_{12} is pair-wise additive ($V_{12} = \sum_{i=1}^{M} v_{12}(\vec{r}_1, \vec{r}_2, \vec{s}_i)$)

$$Q = \frac{1}{2\lambda_1^6}\frac{1}{M!\lambda_2^{3M}}\int e^{-\beta(V_{11}(\vec{r}_1,\vec{r}_2))}d\vec{r}_1 d\vec{r}_2 \left[\int d\vec{s}_1 e^{-\beta v_{12}(\vec{r}_1,\vec{r}_2,\vec{s}_1)}\right]^M. \tag{5}$$

The integral between square brakets is exactly the volume accessible to a single depletant, i.e. the total volume of the system minus the volume prohibited by the presence of the two colloids. Since the depletant-colloid distance can not be smaller than $\frac{\sigma_c+\sigma_p}{2}$, the prohibited volume is twice V_0, the volume of a sphere of diameter $(\sigma_c+\sigma_p)/2$ minus, if the two colloids are close-by, the overlap volume $V_{overlap}$ between the two spheres of diameter $(\sigma_c+\sigma_p)/2$. Thus,

$$\int d\vec{s}_1 e^{-\beta v_{12}(\vec{r}_1,\vec{r}_2,\vec{s}_1)} = V - 2V_0 + V_{overlap}(|\vec{r}_1 - \vec{r}_2|), \tag{6}$$

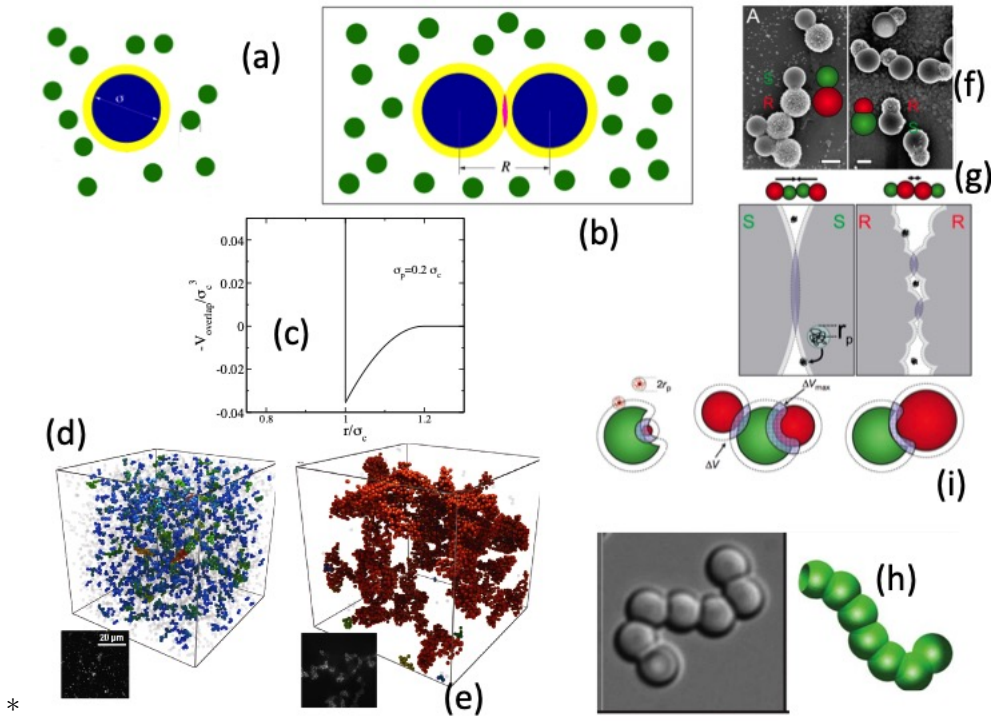

Figure 3: Depletion Interactions: (a) A large colloidal particle immersed in a solution of small particles (usually polymers). The center of the polymer is prevented from accessing the volume occupied by the particle and the corona around it. (b) When two colloidal particles are close-by, the coronas of the two particles overlap increasing the volume accessible to polymers. (c) The shape of the depletion interaction potential calculated by Asakura-Oosawa. (d-e) Confocal images of a colloid polymer mixture for two different polymer concentrations. In (d) the colloids are dispersed in a fluid phase. In (e) the depletion interaction has grown driving the system through a spinodal decomposition process, which leads to the formation of a two-phase system. In the dense phase the dynamics of the particles is strongly reduced, generating a depletion gel. (f-g) Depletion in dumbbells composed by particles with smooth and rough surfaces. The rough surface generates a smaller overlap volume and hence a less intense attraction between rough surfaces as compared to the attraction between smooth surfaces. (i-h) Lock and key colloids. With the appropriate size ratio of the buckled region and the colloidal particle, it is possible to maximize the excluded volume, generating a preferential binding. (h) A colloidal polymer resulting from a lock-and-key depletion mechanism.

where the overlap volume can be calculated geometrically using sphere-sphere intersection properties as

$$V_{overlap}(r) = \frac{\pi}{12}\left[2(\sigma_c + \sigma_p) + r\right]\left[(\sigma_c + \sigma_p) - r\right]^2. \tag{7}$$

Then

$$[V - 2V_0 + V_{overlap}(|\vec{r}_1 - \vec{r}_2|)]^M = (V - 2V_0)^M \left[1 + \frac{V_{overlap}(|\vec{r}_1 - \vec{r}_2|)}{V - 2V_0})\right]^M \tag{8}$$

$$\approx (V - 2V_0)^M \left[1 + M\frac{V_{overlap}(|\vec{r}_1 - \vec{r}_2|)}{V - 2V_0})\right] = (V - 2V_0)^M \left[1 + \rho_M V_{overlap}(|\vec{r}_1 - \vec{r}_2|)\right]$$

where $M/(V - 2V_0) \equiv \rho_M$ is the number density of small spheres. Inserting this result in Eq. 5, it is apparent that the two large colloids interact with a total interaction potential which is the sum of the original HS (V_{11}) potential complemented by an effective potential $V_{eff}(r)$ induced by the presence of the cosolutes whose r dependence is (Fig. 3-(c))

$$V_{eff}(r) = -k_B T \ln[1 + \rho_M V_{overlap}(r)] \approx -k_B T \rho_M V_{overlap}(r) = -\Pi\ V_{overlap}(r), \tag{9}$$

where $\Pi \equiv k_B T \rho_M$ is the ideal gas pressure originating from the cosolutes.

We note on passing that an alternative but equivalent derivation can be formulated in terms of the net force induced by the osmotic pressure on the surface of the two colloids. While when the two large particles are far apart the cosolutes hit the colloids symmetrically, when the two large particles are close-by, the cosolutes are excluded in the overlap volume region, producing a net unbalance in the average pressure which pushes inward the two colloids.

Let's start defining R_d the sum of the colloid and depletant radii, r the center-to-center distance and θ_0 the angle indicated in Fig. 4. From simple geometry we find

$$\frac{r}{2} = R_d \cos\theta_0 \qquad \rightarrow \qquad \cos\theta_0 = \frac{r}{2R_d}$$

We can assume that each surface element $d\vec{a} = R_d^2 \sin\theta d\theta d\phi \hat{a}$ feels a force $d\vec{F}$ coming from the depletants applied (osmotic) pressure Π (applied in R_d, the closest position that depletants can explore)

$$d\vec{F} = -\Pi d\vec{a} = -\Pi R_d^2 \sin\theta d\theta d\phi \hat{a}$$

whose component along the center to center direction x is

$$dF_x = -|d\vec{F}|\ \cos\theta$$

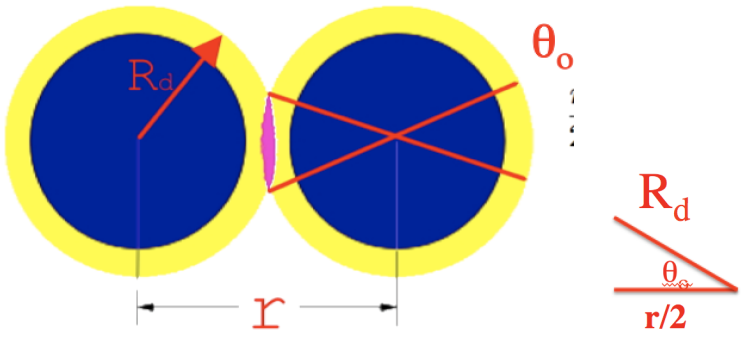

Figure 4: Schematic representation of two colloids (blue) and of the depleted volume (yellow). When the two colloids are close by, the depletion volumes overlaps (purple volume).

Considering that the only unbalanced forces are the one acting inside the angle θ_0 the net force along x can be written as (note that we are integrating over spherical coordinates counting θ from the positive x axis and hence the θ integral goes from 0 to θ_0)

$$F_x(r) = \int_{unbalanced} dF_x = -\Pi R_d^2 \int_0^{2\pi} \int_0^{\theta_0} \cos\theta \sin\theta d\theta d\phi = -\pi\Pi R_d^2 [1-\cos(\theta_0)^2] = -\pi\Pi R_d^2 \left[1 - \left(\frac{r}{2R_d}\right)^2\right]$$

From the force we can evaluate the interaction potential as

$$V(r) = -\int_{2R_d}^{r} F_x(r')dr'$$

$$V(r) = \pi\Pi R_d^2 \int_{2R_d}^{r} \left[1 - \left(\frac{r'}{2R_d}\right)^2\right] dr'$$

giving

$$\frac{V(r)}{\Pi} = -\frac{4\pi R_d^3}{3}\left[1 - \frac{3}{4}\frac{r}{R_d} + \frac{1}{16}\left(\frac{r}{R_d}\right)^3\right] = -V_{overlap}(r)$$

We note that

$$\frac{16 - 12y + y^3}{16} = \frac{(y-2)^2(y+4)}{16}$$

and thus the previous expression can be written, with the change of variable $R_d = \frac{\sigma_c+\sigma_p}{2}$

$$\frac{V(r)}{\Pi} = \frac{4\pi(\sigma_c+\sigma_p)^3}{24}\frac{1}{16}\left(\frac{2r}{\sigma_c+\sigma_p} - 2\right)^2\left(\frac{2r}{\sigma_c+\sigma_p} + 4\right) = \frac{\pi}{12}\left(r - (\sigma_c+\sigma_p)\right)^2\left(r + 2(\sigma_c+\sigma_p)\right)$$

and this expression is identical to the one we had found evaluating the sphere-sphere intersection).

For $\sigma_p \ll \sigma_c$, and defining h as the surface-to-surface distance, both the expression for the force and for the potential simplify, and for $h = r - 2\sigma_c < \sigma_p$ one can approximate $(r + 2(\sigma_c + \sigma_p) \approx 4\sigma_c$ and

$$V(h) = -\Pi \frac{4\sigma_c \pi}{12} (h - \sigma_p)^2$$

and

$$F(h) = -\frac{d}{dh} V(h) = \Pi \pi \frac{2}{3} \sigma_c (\sigma_p - h)$$

Fig. 2.5 Illustration of the overlap volume (*hatched*) of depletion layers between a hard wall and a hard sphere

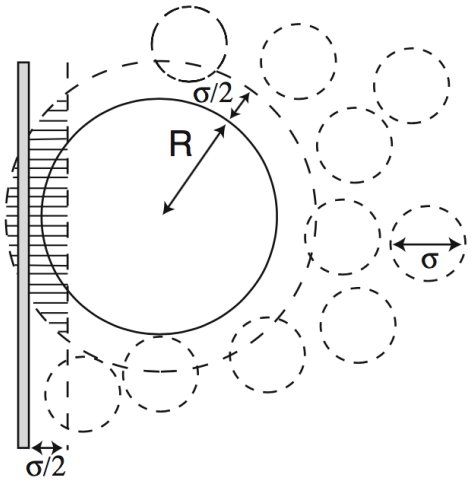

Figure 5: Note that the, along the horizontal axis, the etched surface has a width equal to $\sigma/2 - h$ (on the left of the boundary) and $\sigma/2$ on the right of the boundary. Thus, the cap height is $\sigma - h$. Here h is the distance between the surface and the colloid.

One can similarly treat the case of a hard sphere close to a hard surface, in the presence of depletants. In this case the overlap volume can be calculated by the volume of a spherical cup. Generically, the volume of a cup of height a for a sphere of radius R_0 can be calculated as

$$V_{cup}(a) = \int_0^a \pi z^2 dx$$

and considering that $R_0^2 = z^2 + (R_0 - x)^2$, from which

$$V_{cup}(a) = \int_0^a \pi(2R_0x - x^2)dx = \frac{\pi a^2}{3}(3R_0 - a)$$

In our case, $R_0 = R_d = R + \sigma/2$ and $a = R_d - R - h + \sigma/2 = \sigma - h$ and

$$V_{overlap}(h) = \frac{\pi}{3}(\sigma - h)^2(3R_d - \sigma + h) = \frac{\pi}{3}(\sigma - h)^2(3R + \sigma/2 + h) \qquad 0 < h < \sigma$$

Note that the depletion interaction is attractive. Hence if we put a colloidal solution in a vessel containing some small surfactant, the spacial distribution of the colloidal particles will be altered. Particles will tend to explore more frequently the boundary of the sample. Playing with the geometry of the sample holder, it is possible to push the colloids in specific locations. Fig. 5.1 shows graphically that a colloidal particles is driven toward inner corners, since in that configuration the excluded volume is maximized.

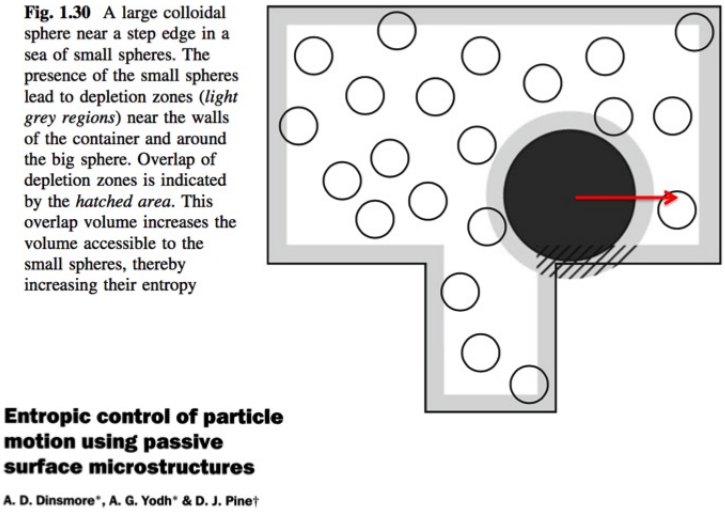

Fig. 1.30 A large colloidal sphere near a step edge in a sea of small spheres. The presence of the small spheres lead to depletion zones (*light grey regions*) near the walls of the container and around the big sphere. Overlap of depletion zones is indicated by the *hatched area*. This overlap volume increases the volume accessible to the small spheres, thereby increasing their entropy

Entropic control of particle motion using passive surface microstructures

A. D. Dinsmore*, A. G. Yodh* & D. J. Pine†

5.2 wall-wall case

We conclude this series of calculation looking at the wall-wall case.

In this case, if the distance between the planes of surface A is less than σ_p, there are no depletants between the two walls. Hence the internal pressure is zero, while the outside pressure is always $P = \rho_p k_B T$. Then

$$F(h) = PA$$

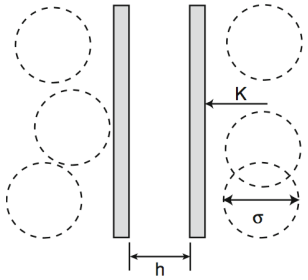

Fig. 2.1 Schematic picture of two parallel flat plates in the presence of penetrable hard spheres (*dashed circles*)

and

$$V(h) = -\int_{\sigma}^{h} F(h')dh' = -PA(h-\sigma) \qquad 0 < h < \sigma$$

We can also check the Derjaguin approximation which states that for $h << R$

$$F_{sphere-sphere} = \pi R W_{plane-plane}$$

In the depletion interaction case, for $h << R$, we have seen that

$$F_{sphere-sphere} = P\pi R(\sigma - h) \qquad W_{plane-plane} = -PA(h-\sigma)$$

consistent with the Derjaguin approximation.

5.2.1 Application of depletion interactions

The essence of the depletion interaction is the tiny gain of entropy experienced by each cosolute when colloids are close-by (and $V_{overlap}$ is different from zero), originating from the possibility to additionally explore the overlap volume. This entropy gain, once multiplied by the large number M of small cosolutes, results into a net attractive potential between the two colloids, which can easily become of the order of the thermal energy k_BT. The concentration of cosolutes then determines the strength of the interaction while their size determines the interaction range, explaining the large versatility of depletion interaction in the design of effective potentials between colloids.

Depletion forces have found several applications in colloidal science

- to induce crystallization, phase separation, shape fractionation. The ability to control the interaction range has been exploited to investigate the existence of the liquid state, colloidal gelation(Fig. 3-(d-e)), glass-glass transitions.
- to control the self-assembly of dumbbells composed by fused spheres of different surface roughness(Fig. 3-(f-g)) The different overlap volume between rough and smooth spheres and between locks and keys of comparable size is the crucial element in the self-assembly process.

- to control the self-assembly of colloidal particles with indented surfaces(Fig. 3-(h-i)), to imitate the lock and key mechanism of protein selectivity.
- to direct the motion of colloidal particles on properly patterned surfaces or to drive crystallization on patterned surfaces.
- to provide a depletion analog of critical Casimir forces. Recently, depletion interactions arising from highly polydisperse cosolutes clusters, typical of systems in proximity of a sol-gel transition, have been evaluated numerically. The observed exponential attractive effective potential and the tunable range of the interaction (depending on the distance from percolation) suggests a similarity with critical Casimir forces.

5.3 Biological Evidence: Clustering of Red Blood Cells: Lekkerkerker-Tunier

Red blood cells (RBCs) are biconcave particles and their detailed shape and size depend on the RBC type. The human RBC may be considered a disc with a diameter of 6.6 μm and a thickness of 2 μ nm; its volume thus being of the order of 70 μm^3: The RBCs occupy about 40 to 50 vol % of our blood.

Already in the 18th century it was known that RBCs tend to cluster, preferably with their flat sides facing each other. Such a side by side RBC aggregate reminds of the packing of 'a number of coins'. These structures are commonly denoted as "rouleaux". In blood of healthy human beings the tendency of RBCs to aggregate is weak. In case of pregnancy or a wide range of illnesses aggregation is found to be enhanced, giving rather pronounced rouleaux, see Fig. 1.11.

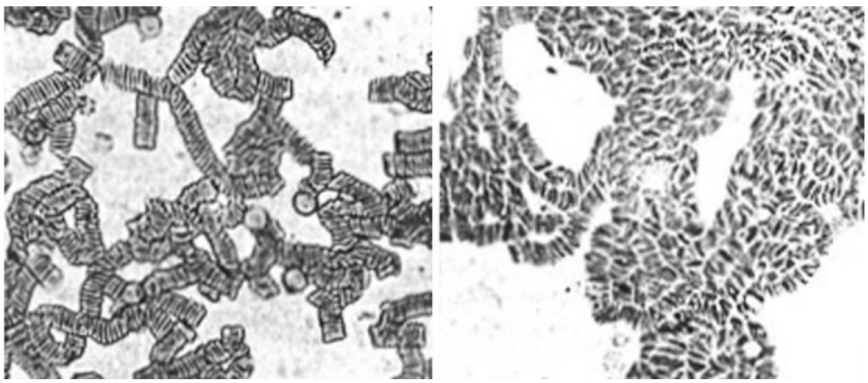

Fig. 1.11 Red blood cells in healthy blood (*right*) exhibiting weak aggregation and in blood of a pneumonia patient (*left*) in which rouleaux formation took place (strong aggregation) [67]. Picture reprinted from R. Fåhraeus, *Physiol. Rev.*, 9:241, Copyright 1929, with permission from APS

Enhanced RBC aggregation can be detected for instance by measuring the sedimentation rate. The sedimentation rate varies between 1 and 3 mm/h for healthy blood up to 100 mm/h in case of severe illnesses. The blood sedimentation test, based on monitoring aggregation of red blood cells, became a standard method for detecting illnesses. The relation between pathological condition, RBC aggregation and enhanced sedimentation rate, has been known for at least two centuries. Fähraeus related enhanced aggregation of RBCs plus longer and stronger rouleaux to the concentration of the blood serum proteins fibrinogen, globulin and albumin. The tendency to promote aggregation depends on the type of protein. Rouleaux formation is most sensitive to increased serum concentrations of (rod-like) fibrinogen (molar mass 340 kg/mol) compared to (globular) β- and γ-globulins (90 and 156 kg/mol, respectively). The globulins in turn lead to RBC aggregation at lower protein concentrations than albumin proteins (69 kg/mol). It has further been shown that adding other macromolecules such as dextrans also promote rouleaux formation. Asakura and Oosawa (whose theory we will discuss later on) suggested that RBC aggregation might be caused by depletion forces between the RBCs induced by serum proteins. This is in line with the finding that the sedimentation rate is more sensitive to larger serum proteins. Some authors interpret rouleaux formation as being caused by bridging of RBCs by serum proteins. There is however no evidence for protein adsorption onto RBCs. A study on rouleaux formation in mixtures of human RBCs (diameter 6.6μm) and rabbit RBCs (diameter 7.8 μm) resulted in rouleaux structures that consisted (mainly) of only a single type of RBC. This can be explained by a depletion effect (the overlap volume, hence entropy, is maximized if similar RBCs stack onto each other). In case of bridging, however, mixed aggregates are expected, so there is little support for the bridging hypothesis. **The general picture is that red blood cells tend to cluster at elevated concentrations of the blood serum proteins, which act as depletants.**

5.4 Mixing Biopolymers

Another manifestation of a depletion phenomenon was reported by the micro-biologist Beijerinck who tried to mix gelatin (denatured protein coil) with starch (polysaccharide) in aqueous solution in order to prepare new Petri dish growth media for bacteria. He reported that these biopolymers could not be mixed; "emulsion droplets" appeared instead. With current knowledge this can be regarded as an early detection of depletion-induced demixing. The separate liquid phases in demixed protein-polysaccharide mixtures can sometimes be characterized by a sharp liquid-liquid interface. The interfacial tension between the coexisting phases in protein-polysaccharide mixtures has been determined and is of the order of μN/m.

5.5 Depletion Effects in Biological Systems: Macromolecular Crowding

A longstanding question in molecular biology is the extent to which the behaviour of macromolecules observed in vitro accurately reflects their behavior in vivo. The cytoplasm of a living cell contains a high concentration of macro-molecules (up to 400 g/L), including proteins and nucleic acids. Over the last 30 years or so it has been increasingly appreciated that the large volume fraction occupied by these macromolecules influences several intracellular processes, ranging from the bundling of biopolymers like DNA and actin to the phase separation in a bacterial cell. These effects are known amongst biochemists and biophysicists as macromolecular crowding.

Phase separation between a nucleoid and cytoplasm in bacterial cells is a striking example of macromolecular crowding. Chromosomes in bacterial cells do not occur in dispersed form but are organized in the nucleoid as a separate phase. Depletion forces that originate from the presence of proteins can explain the phase separation. As a result, the proteins partition over the cytoplasm and nucleoid phases. Their concentration in the cytoplasm is about two times larger than their concentration in the nucleoid phase (see Figs. 1.24).

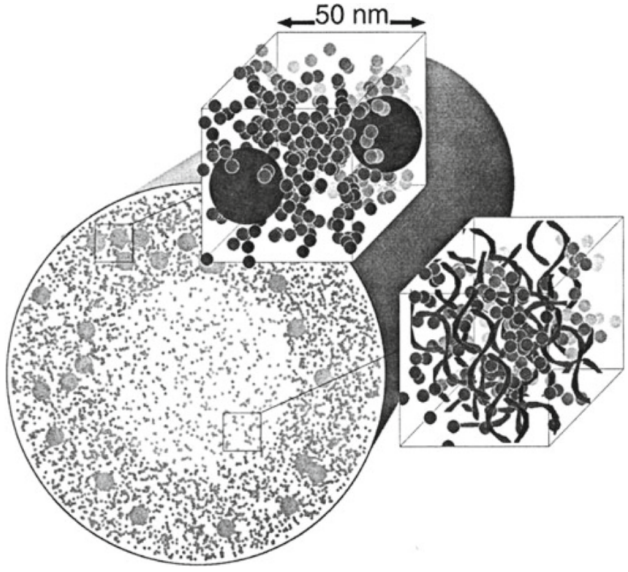

Fig. 1.24 Schematic picture of a cell containing phase separated nucleoid (cube on the *right*; magnifies DNA (*chains*) and proteins (*small spheres*) in this phase) and serum (*upper cube*; containing proteins and ribosomes as *big spheres*). Sketch by Woldringh and Odijk [255]. Reprinted from C. L. Woldringh and T. Odijk *in: Organization of the Prokaryotic Genome, R. L. Charlebois (Ed.)*. ASM Press, Amsterdam, Copyright 1999, with permission from ASM Press

Depletion forces can be of use in biomedical applications. Non-adsorbing polymer chains promote the adhesion of cells to surfaces and enhance adsorption of lung surfactants at the

air/water interface in lungs so as to help patients suffering from acute respiratory syndrome. The physical properties of actin networks are affected by non-adsorbing polymers, which also modify phase transitions in virus dispersions.

5.6 Combinatorial Entropy: microemulsion droplets linked by telechelic polymers

Another source of entropy, different from the translational, orientational, or depletion cases we have previously discussed, plays an important role in soft matter self-assembly processes. This entropy arises from the different combinatorial ways one can distribute bonds between distinct clusters. One interesting case is offered by a solution of microemulsion droplets linked by telechelic polymers.The two hydrophobic ends of each polymer are energetically constrained to reside inside the oil droplets, in the same or in two different ones. Thus, the polymers can provide links between different droplets. To a first approximation, energy does not play a relevant role and the behaviour of the system is mainly controlled by the different ways the polymer ends can be distributed over the accessible droplets.

Ideally, since all ends must be inside oil droplets, one would think that the state of maximum entropy is the one in which both ends of the polymers reside in the same droplet (Fig. 6-(a)). Indeed, in this configuration all droplets retain their translational freedom. Binding between droplets to generate a connected structure (Fig. 6-(b)) would imply a loss of translational entropy. This simple argument neglects the fact that the possibility to connect with neighbouring droplets significantly increases the number of microstates so much to overcome, beyond a certain packing fraction and beyond a certain number of polymers per droplet, the loss of translational entropy upon binding.

A theoretical analysis of this system, highlighting the importance of the combinatorial entropy has been presented by Safran and coworkers. The authors propose to write a zero-order free energy as a function of two independent parameters: the droplet concentration $\rho_d = \frac{N}{V}$ and the polymer concentration $\rho_p = \frac{N_p}{V}$. By neglecting coupling between the droplets and the polymers, the free energy can be expressed as $\beta F = \beta F_{droplet} + \beta F_{polymer}$, where

$$\beta F_{polymer} = -N_p \ln Z_p \quad \text{with} \quad Z_p = N \frac{\Sigma_d}{\Sigma_p} \left(\frac{\Sigma_d}{\Sigma_p} + N_d^{accessible} \frac{\Sigma_d}{\Sigma_p} \right). \tag{10}$$

Here $N_d^{accessible} \sim \rho_d$ indicates the number of droplets that can be connected by a polymer originating in an arbitrary selected droplet. Note that we have assumed that $\frac{\Sigma_d}{\Sigma_p}$ is the number of attachment points on a droplet (proportional to the surface area Σ_d of the droplet divided by the surface area Σ_p of the polymer head). Each polymer can then end on the same droplet with probability $\frac{\Sigma_d}{\Sigma_p}$ and on a distinct but accessible droplet with probability $N_d^{accessible} \frac{\Sigma_d}{\Sigma_p}$. Note that the polymer free energy does not incorporate any energetic contribution.

The system is thermodynamically stable if the free energy is a convex function of both

ρ_p and ρ_d. This means that the second derivative of the free energy ($\delta^2 F = F_{\rho_d,\rho_d}\delta\rho_d^2 + 2F_{\rho_d,\rho_p}\delta\rho_d\delta\rho_p + F_{\rho_p,\rho_p}\delta\rho_p^2$) has to be positive. Equivalently, the matrix

$$\begin{pmatrix} F_{\rho_d,\rho_d} & F_{\rho_d,\rho_p} \\ F_{\rho_d,\rho_p} & F_{\rho_p,\rho_p} \end{pmatrix} \tag{11}$$

must posses two positive eigenvalues, allowing us to separate stable from unstable states (mean field spinodals). The results of the calculations for different values of the number of polymers per droplet r are shown in Fig. 6-(d) and compared with the corresponding experimental data (Fig. 6-(c)). Beyond a critical value of r, at low densities the system prefers to phase separate in a gas phase of droplets, in which polymers start and end in the same droplet, and in a connected phase (a network) in which the ends of the polymer preferentially explore the interior of different droplets. The connected phase emerging from the entropic phase separation constitutes a dense gel phase, being the number of connections per droplet significantly larger than the percolation threshold.

5.7 Combinatorial Entropy: DNA grafted particles

Another interesting and very recent application, where combinatorial entropy plays an important role in controlling attraction between particles, is found in DNA grafted colloids. These are gold (at the nanoscale) or polymeric particles coated with DNA strands [**?**, **?**, **?**]. The DNA strands end with a specific sequence $\mathcal{A}$ (sticky end) that can bind to complementary sequences $\bar{\mathcal{A}}$ on nearby coated colloids.

If the particles are grafted with both $\mathcal{A}$ and $\bar{\mathcal{A}}$ sticky ends [**?**, **?**] (or if $\mathcal{A}$ is self complementary and, thus, able to bind to itself satisfying the Watson-Crick pairing rules) the situation is analogous to the microemulsion droplets linked by telechelic polymers [**?**] is encountered. Indeed particles can always satisfy their bonds (exploiting intra or inter particle links), rendering the energetic contribution to binding irrelevant [**?**]. In this case, again, only the combinatorial contributions dictate the net attraction between the particles. This is quite relevant since, for several-bases long sticky sequences, the binding energy can easily become dozens of k_BT which would suggest at a first glance an irreversible aggregation process. Differently, the combinatorial term can be tuned to be of the order of a few k_BT, making a reversible self-assembly process possible, especially if the bonding scheme is associated to a toehold displacement mechanism [**?**].

To clarify the role of combinatorial entropy in the case of palindromic DNA sticky sequences $\mathcal{A} = \bar{\mathcal{A}}$, consider the case of two particles with grafted polymers ending with a sticky site that can bind to only one other distinct sticky site (see Fig. 7). When the particles are far, all sticky sites find their own partner among chains grafted on the same particle. At low T, all sticky sites are essentially paired. One would then expect that under these conditions there is no additional energetic gain that can compensate for the loss of translational entropy upon inter-particle binding. Instead, when the particles probe

distances x compatible with intra-particle binding (see Fig. 7) a finite number $B(x)$ of chains on each particle can bind to partners grafted on the other particle.

To estimate the strength of the entropic attraction let us focus on this pool of approximatively $2B(x)$ interacting sites, which can pair to form $B(x)$ bonds. If each site can bind to any other site, independently from where the corresponding chain is grafted, then the number of distinct bonding patterns is $(2B(x)-1)!!$ (being !! the symbol for double factorial). Indeed the first site can bind to $2B(x)-1$ other sites, the first of the remaining $2B(x)-2$ sites can bind to $2B(x)-3$ others and so on, resulting in the double factorial term. If instead a site can only bind to sites of the same particle, then the number of distinct bonding configurations is $(B(x)-1)!!$ for each particle. Thus, the change in entropy introduced from allowing inter-particle binding can be quantified as

$$\frac{\Delta S^{comb}(x)}{k_B} = \ln\left[\frac{(2B(x)-1)!!}{[(B(x)-1)!!]^2}\right]. \tag{12}$$

For typical nanoparticles grafting densities, $B(x) \sim 5-25$, corresponding to entropic attraction $\Delta S^{comb}/k_B \sim 2.7-16$. Such entropic contribution is sufficient to compensate the repulsive contribution arising from the overlap between the brushes, and to provide a net attractive potential sufficiently strong to drive aggregation of the colloidal particles into a dense liquid or into a crystal phase.

6 Riguardiamo in generale cosa abbiamo fatto: il concetto di potenziale efficace

Supponiamo di avere un sistema composto da N particelle "lente" o "grandi" e M particelle "veloci" o "piccole". La funzione di partizione del sistema e' data da

$$Q_{N+M} = \frac{1}{N!\lambda_N^{3N}}\frac{1}{M!\lambda_M^{3M}}\int d\vec{r}_1...d\vec{r}_N\int d\vec{s}_1...d\vec{s}_M e^{-\beta(V_{11}(\vec{r}^N)+V_{12}(\vec{r}^N,\vec{s}^M)+V_{22}(\vec{s}^M)}$$

possiamo formalmente scrivere

$$e^{-\beta V_{eff}(\vec{r}^N)} = \frac{1}{M!\lambda_M^{3M}}\int d\vec{s}_1...d\vec{s}_M e^{-\beta(V_{12}(\vec{r}^N,\vec{s}^M)+V_{22}(\vec{s}^M)}$$

cosi' che

$$Q_{N+M} = \frac{1}{N!\lambda_N^{3N}}\int d\vec{r}_1...d\vec{r}_N e^{-\beta V_{11}(\vec{r}^N)}e^{-\beta V_{eff}(\vec{r}^N)}$$

per cui il potenziale del sistema formato dalle particelle "grandi" e'

$$V_{tot}(\vec{r}^N) = V_{11}(\vec{r}^N) + V_{eff}(\vec{r}^N)$$

dove pero' $V_{eff}(\vec{r}^N)$ e' funzione della temperatura e della densita'. Infatti.. possiamo gia' velocemente vedere che

$$-\beta V_{eff}(\vec{r}^N) = \ln \frac{V^M}{M!\lambda_M^{3M}} + \ln\left(\frac{Z(\vec{r}^N)}{V^M}\right) = -V[\rho_M \ln(\rho_M \lambda_M^3) - \rho_M] + \ln\left(\frac{Z(\vec{r}^N)}{V^M}\right)$$

con

$$Z(\vec{r}^N) = \int d\vec{s}_1 ... d\vec{s}_M e^{-\beta V_{22}(\vec{s}^M)} e^{-\beta V_{12}(\vec{s}^M, \vec{r}^N)}$$

Fin qui, non abbiamo fatto nessuna approssimazione, e la media di qualsiasi quantita' dipendente da $\vec{r}^N$ solo, usando $V_{tot}(\vec{r}^N)$ nella funzione di partizione e' esatta.

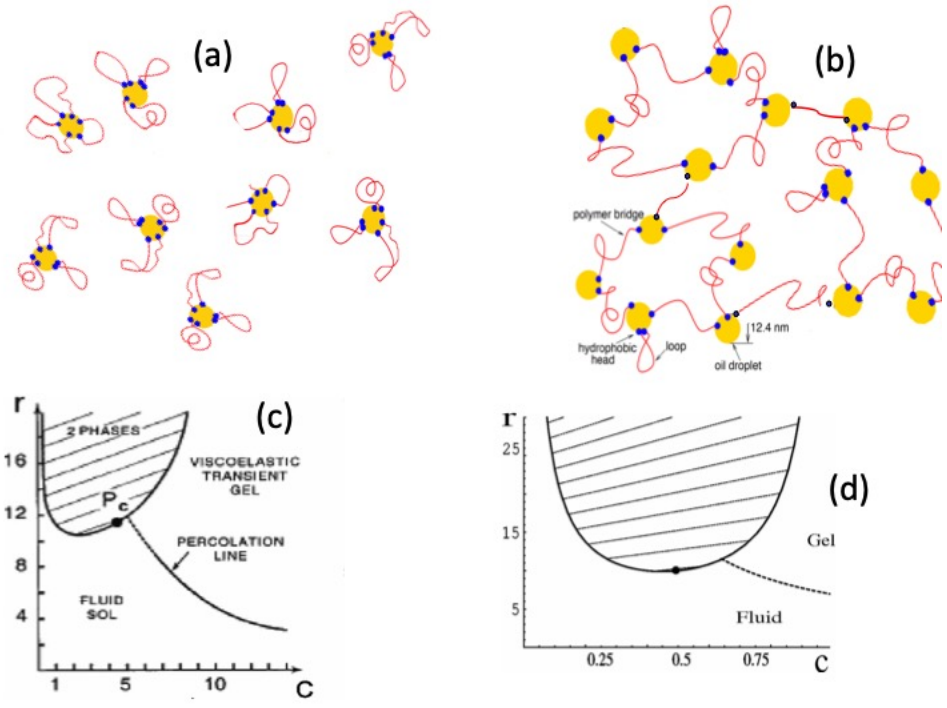

Figure 6: Cartoon of the microemulsion droplets (yellow spheres) connected by telechelic polymers (red) with hydrophobic ends (blues). (a) A schematic representation of a gas-like phase in which both ends of the polymers are immersed in the same droplet. (b) A dense percolating liquid-like phase, in which polymers connects different droplets. (c) Experimental phase diagram showing a phase-coexistence between a dilute and a dense phase of droplets, induced by the increase in the number of polymers per droplet r. (d) Theoretical phase diagram.

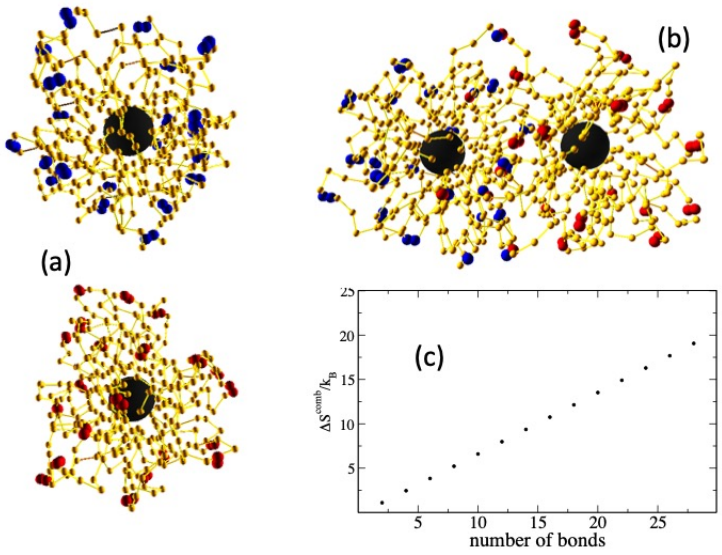

Figure 7: Cartoon of a nanoparticle (black) decorated by grafted polymers ending with a sticky sequence (blue and red, respectively). (a) Two isolated particles in which all sticky ends form intraparticle bonds. (b) Two close-by particles in which some of the bonds involve chains of different particles (red-blue pairs). (c) Combinatorial entropy change associated to the formation of interparticle bonds.